Available online at www.sciencedirect.com
ScienceDirect
Geochimica et Cosmochimica Acta 71 (2007) 2858–2875
Geochimica et Cosmochimica Acta
www.elsevier.com/locate/gca

An experimental study on the hydrothermal preparation of tochilinite nanotubes and tochilinite–serpentine-intergrowth nanotubes from metal particles

Yiya Peng [a,b,c,*], Liqiang Xu [a], Guangcheng Xi [a], Chang Zhong [a,1], Jun Lu [a], Zhaoyu Meng [a], Gongpu Li [b], Shuyuan Zhang [b], Gangya Zhang [d], Yitai Qian [a,b]

[a] Department of Chemistry, University of Science and Technology of China, Hefei, Anhui 230026, PR China
[b] Structure Research Laboratory, University of Science and Technology of China, Hefei, Anhui 230026, PR China
[c] Department of Chemistry, Zhengzhou University, Zhengzhou, Henan 450052, PR China
[d] Institute of Soil Science, Chinese Academy of Sciences, Nanjing, Jiangsu 210008, PR China

Received 4 May 2006; accepted in revised form 21 March 2007; available online 27 March 2007

Abstract

Tochilinite and tochilinite–serpentine-intergrowth (TSI) phases, including their nanotubes, are major components of CM carbonaceous chondrites. The laboratory synthesis of tochilinite and TSI phases, particularly their nanotubular forms, has rarely been reported. In this article, we show that FeMgAl tochilinite nanotubes and TSI nanotubes can be hydrothermally prepared from heat-treated metal particle mixtures below 200 °C under reducing and basic conditions. The metal particles used in the preparation of FeMgAl tochilinite were Fe, Mg and Al and those used for the preparation of TSI were Fe, Mg, Al, Si, Cr and Ni. FE-SEM, TEM, HRTEM, ED, EDX and XRD were used to characterize the reaction products. The yield of FeMgAl tochilinite and TSI was generally low and the FeMgAl tochilinite and TSI samples were very heterogeneous. Both the FeMgAl tochilinite and TSI crystallites existed in two forms, i.e. flakes and nanotubes. They generally had micrometer to sub-micrometer sizes and low crystallinity, and they were extremely sensitive to the electron beam. The FeMgAl tochilinite showed various structural modifications; however, the chemical compositions of these structural modifications were similar. The same phenomenon existed for TSI. The structural modifications of FeMgAl tochilinite and TSI may originate mainly from their mixed-layer structures, two-dimensional incommensurability of their sub-structures and the synthetic conditions. Some of the FeMgAl tochilinite nanotubes and the TSI nanotubes were likely to have been formed by curling of the corresponding flakes. The curling process appears to be delicate, requiring a quiet reaction environment with stable temperature and pressure and without vibrations. Our synthetic FeMgAl tochilinite and TSI showed remarkable similarities to natural tochilinite and TSI, respectively. Therefore, meteoritic tochilinite and TSI probably formed by reaction of metal particles with S^{2-} bearing water at temperatures of around 50–100 °C.
© 2007 Elsevier Ltd. All rights reserved.

1. INTRODUCTION

In the past decade, inorganic nanotubes have been widely studied and various methods have been employed to prepare these microscopic materials (Tenne and Rao, 2004). However, two long-known inorganic nanotubular materials—tochilinite and tochilinite–serpentine-intergrowth (TSI) nanotubes—have rarely been studied (Tomeoka and Buseck, 1983, 1985; Bradley and Brownlee, 1991;

* Corresponding author.
E-mail address: wypeng@zzu.edu.cn (Y. Peng).
[1] Present address: Department of Chemistry, Northwestern University, Evanston, IL 60208-3113, USA.

0016-7037/$ - see front matter © 2007 Elsevier Ltd. All rights reserved.
doi:10.1016/j.gca.2007.03.012

Kakos et al., 1994). These two kinds of nanotubes were first identified in CM carbonaceous chondrites about 25 years ago (Tomeoka and Buseck, 1983, 1985), and later (1991) in interplanetary dust particles (IDPs) (Bradley and Brownlee, 1991). Tochilinite microtubes were also found in terrestrial mines (Zolensky and Mackinnon, 1986). TSI nanotubes or microtubes have not been found in terrestrial mines though they probably exist (Zolensky and Mackinnon, 1986).

The mineral name, tochilinite, represents a mineral group exhibiting ordered mixed-layer structure and containing an alternating pattern of metal sulfide layers with mackinawite-like structure and metal hydroxide layers with brucite-like structure (Organova et al., 1974; Mackinnon and Zolensky, 1984; Zolensky, 1987). According to Organova et al. (1974), at least four kinds of tochilinite have been identified: tochilinite I, tochilinite II, phase I and phase II. Special attention should be paid to the metal elements of the brucite-like layers of the four kinds of terrestrial tochilinite: only Mg and Fe exist, while other elements such as Al, Ca, Cr, etc are not present. However, these elements appear in other terrestrial tochilinites, as documented in the work of Kakos et al. (1994). Although the tochilinite structures can be described using large superlattices, they are more conveniently defined by two separate sublattices, the sulfide component and the hydroxide component (Organova et al., 1974; Kakos et al., 1994).

The TSI structure is considered to be an intergrowth of serpentine-type layers and tochilinite-like layers (Mackinnon and Zolensky, 1984; Zolensky et al., 1993; Nakamura and Nakamuta, 1996). The serpentine mineral group includes individual minerals such as chrysotile, lizardite, antigorite and cronstedtite (Kogure et al., 2001; Dódony and Buseck, 2004). Therefore, if the TSI was assumed to have a 1:1 intergrowth of serpentine-type layers and tochilinite-like layers (a serpentine–tochilinite–serpentine–tochilinite or S–T–S–T intergrowth mode), then theoretically, several kinds of TSIs would be produced by various assemblages of the four kinds of tochilinite and individual serpentine minerals. However, it is probable that only part of these assemblages can exist in practice. To date, no attempt has been made to determine this possibility. Like the structure of tochilinite, it might be convenient to use separate sublattices to describe the structure of TSI.

Tochilinite and TSI, especially their nanotubes, are important minerals that constitute the matrix and fine-grained chondrule rims (FGRs) of CM carbonaceous chondrites and IDPs (Tomeoka and Buseck, 1983, 1985; Mackinnon and Zolensky, 1984; Zolensky, 1987; Bradley and Brownlee, 1991; Zolensky et al., 1993; Nakamura and Nakamuta, 1996). However, very little has been reported on the laboratory synthesis and theoretical study of tochilinite phases (Kakos et al., 1994; Browning and Bourcier, 1996; Kozerenko et al., 1996, 2001; Moroz et al., 1997; Rusakov et al., 1998; Chistyakova et al., 2005). Moreover, no literature exists on the laboratory preparation of TSI and its nanotubes. In this article, we show that FeMgAl tochilinite (Kakos et al., 1994) and TSI, especially their nanotubular forms, can be hydrothermally prepared from heat-treated metal particle mixtures at temperatures below 200 °C under reducing and basic conditions. The applications of our experimental results to meteoritics are discussed.

2. MATERIALS AND INSTRUMENTATION

2.1. Preparation of the metal particle precursor mixture (MPPM)

The purity and sizes of the metal particles used in this study are listed in Table A1 in the Appendix. All metal powders were purchased from Shanghai Chemical Reagents Company. The metal particle precursor mixture (MPPM) of FeMgAl tochilinite and TSI were prepared in either an H_2 or Ar atmosphere. A typical procedure follows: 7.5 g Fe (0.13 mol), 2.5 g Mg (0.10 mol) and 2 g Al (0.07 mol) powders were mixed homogeneously and pressed into pellets. The pellets were heated in an H_2 atmosphere at 500 °C for 5 h to remove possible surface oxides of the transition metal particles and then the temperature was increased to 750–860 °C. The pellets were kept at this temperature for another 2–3 h to ensure close contact between the metal particles (the melting points of Mg and Al are 648.8 and 660.4 °C, respectively). If an Ar atmosphere was used, the pellets could be heated directly to 760–860 °C and kept at this temperature for 2–3 h. After cooling to room temperature, the pellets were made into millimeter to micrometer-sized powders using a hammer. The MPPM of TSI was prepared similarly using metal powders of 10 g Fe (0.18 mol), 5 g Si (0.19 mol), 4 g Mg (0.17 mol), 3 g Al (0.11 mol), 1.5 g Ni (0.03 mol) and 0.5 g Cr (0.01 mol). X-ray diffraction (XRD) analysis of the MPPMs showed that some alloying might have occurred.

The elemental ratios of the FeMgAl tochilinite MPPM were derived from Kakos et al. (1994). However, we increased the Mg and Al contents a little to ensure close contact between Fe particles and metallic Mg and Al, which was originally assumed to be beneficial for the preparation of FeMgAl tochilinite. Similarly, the elemental ratios of the TSI MPPM were derived from Bradley and Brownlee (1991), with a substantially increased amount of Mg, Al and Si. The reason that we used more Mg, Al and Si to perform the synthesis was based on the fact that metallic Mg, Al and Si react more quickly than Fe, Ni and Cr in a hydrothermal environment. In order to lessen the supposed reaction segregation (i.e. the tendency for the active elements to react first to form stable phases other than FeMgAl tochilinite and TSI, and the inactive elements to react later), we used more Mg, Al and Si metal powders.

2.2. Instrumentation

Field-emitting scanning electron microscopy (FE-SEM), transmission electron microscopy (TEM), High-resolution transmission electron microscopy (HRTEM), Energy-dispersed X-ray spectroscopy (EDX), electron diffraction (ED) and XRD were utilized in this study. The FE-SEM observations were performed on a JEOL field-emitting scanning electron microscope (JEOL JSM-6300F) and an FEI Sirion field-emitting scanning electron microscope

(FEI company). The samples for FE-SEM observation were gold coated. TEM observations were performed on a Hitachi H-800 TEM, a JEOL 2010 TEM and a JEOL 2010F TEM, all working at an accelerating voltage of 200 kV. The JEOL 2010F TEM was associated with an INCA Energy EDX system from Oxford Instruments and the JEOL 2010 TEM an Oxford Link ISIS EDX system. The JEOL 2010 TEM and the JEOL 2010F TEM had CCD cameras, thus some of the TEM images shown in this paper were obtained from CCD cameras, while others were obtained from negatives. HRTEM images were obtained on the JEOL 2010 TEM. EDX analysis was performed on both JEOL 2010F and JEOL 2010 TEM after depositing the ultrasonicated samples in ethanol on amorphous carbon film coated copper TEM grids. EDX data presented in this paper were all from the more advanced INCA Energy EDX system associated with the JEOL 2010F TEM that had a field emission gun. However, these data are also representative of those obtained on the Oxford Link ISIS EDX system. The EDX analysis was a standard free analysis, therefore, the results given in this paper should be considered as having an accuracy no better than 0.1% (W/W). The element quantitation method is Cliff-Lorimer thin film approximation with XPP matrix correction. The XPP method is more accurate than old methods (e.g. ZAF method), particularly for light elements. XRD patterns were recorded with a MAX 18 AHF X-ray diffractometer (MAC Science Co. Ltd) with Cu-Kα_1 radiation ($\lambda = 1.54056$ Å). The contents of the metal elements in the samples were determined by inductively coupled plasma-atomic emission spectroscopy (ICP-AES), which was performed on an Atomscan Advantage spectrometer (Thermal Jarrel Ash Corp.).

3. HYDROTHERMAL SYNTHESIS OF FEMGAL TOCHILINITE AND TSI

3.1. Introduction and design of the hydrothermal experiment

It has previously been reported that a reductive and basic environment is necessary for the hydrothermal preparation of tochilinite (Kakos et al., 1994; Browning and Bourcier, 1996; Kozerenko et al., 1996, 2001; Moroz et al., 1997). In order to find the optimum reaction conditions to increase the yield of FeMgAl tochilinite and TSI, it is worthwhile to determine why a reducing environment is needed. Of course, the hydroxide components of tochilinite and TSI naturally require a basic environment for their formation. The mineral valleriite has a similar structure to tochilinite (Organova et al., 1974). Evans and Allmann (1968) and Hughes et al. (1993) postulate that the hydroxide layer in valleriite possesses positive charges and the sulfide layer contains (delocalized) negative charges. We think that this scenario may also apply to the structure of tochilinite. Thus, the hydroxide layer in tochilinite probably also contains positive charges. The Fe–S layer in mackinawite has been calculated to be metallic and the calculation is based on an ideal mackinawite structure (Welz and Rosenberg, 1987). Although the structure of the Fe–S layer in tochilinite is different from that of mackinawite (Organova et al., 1974; Lennie et al., 1995), if one omits this difference, one reaches the tentative conclusion that the Fe–S layer in tochilinite might contain negative charges. Based on the above considerations, it can be inferred that if tochilinite was to form, electrons should be injected into the Fe–S layer to compensate for the positive charges that reside on the hydroxide layer. Thus, a reducing environment will be necessary if tochilinite is to form. It can be further deduced that if more electrons can get into the sulfide layers of tochilinite or valleriite, the sulfide layers will need more hydroxide components to compensate for their negative charges. Therefore, more tochilinite or valleriite potentially will be produced. This scenario may also apply to the synthesis of TSI.

The best way to supply electrons in a hydrothermal environment is to increase the reaction system's reducing strength. Based on this assumption, we designed three kinds of experiments to be used in this study. The reducing strength of the three kinds of experiments is varied; hence, we could study the relationship between the reducing strength of the reaction system and the yield of FeMgAl tochilinite and TSI. The main feature of the first set of experiments was to perform the related operations, like weighing the reagents and loading the autoclaves, in a glovebox filled with high-purity N_2 or Ar, completely excluding the effect of O_2. In this way, the reducing strength of the reaction system was self-generated. The second set of experiments was based on the first. In this case, not only were the related operations performed in an inert atmosphere but the autoclaves were also flushed with H_2 before closing, a technique similarly applied by Kakos et al. (1994). In the third set of experiments, aqueous hydrazine monohydrate ($N_2H_4{\cdot}H_2O$), a strong reducing agent, was added into the reaction system (Mellor, 1958). Hydrazine monohydrate has also been used to supply electrons to transition metal dichalcogenide layers in aqueous solutions (Schöllhorn et al., 1975), and it has effects similar to the cathodic reduction method (Schöllhorn and Meyer, 1974). We ultimately discovered that the third set of experiments was more effective in producing FeMgAl tochilinite and TSI; therefore, this paper is based on these experimental findings.

3.2. Details of the hydrothermal experiment

Two kinds of sulfur sources were used to prepare FeMgAl tochilinite and TSI. One was $(NH_4)_2S$ aqueous solution (8%, w/w), the other was elemental sulfur. As elemental sulfur can be easily reduced to hydrogen sulfide and ammonium sulfide by hydrazine monohydrate (Mellor, 1958), we used it as the sulfur source in parts of the synthetic experiments employing hydrazine monohydrate.

Both stainless steel (US 304 stainless steel) autoclaves and Teflon-lined stainless steel autoclaves of 50 mL capacity were used to prepare FeMgAl tochilinite (the inner diameters of the autoclaves were about 2.9 cm and the heights were about 8 cm). Only stainless steel autoclaves were used to prepare TSI. Our Teflon-lined stainless steel autoclaves do not withstand temperatures higher than 185 °C for a long time. An electric stove, able to gradually

rise in temperature from 22 to 200 °C over the course of 5 h, was used in all the experiments. All operations, including weighing of the reagents and loading of the autoclaves, were performed in a glovebox in flowing high-purity N_2 or Ar. In a typical preparation run of FeMgAl tochilinite or TSI, 0.3 g MPPM, 4.0–6.0 mL saturated $(NH_4)_2S$ aqueous solution (8%, w/w) (or 0.18–0.28 g elemental sulfur), 18 mL $N_2H_4{\cdot}H_2O$ aqueous solution (85%, v/v) and 0.40 g NaOH (or 0.42 g $LiOH{\cdot}H_2O$) were placed into an autoclave. The MPPM was suspended in the middle part of the autoclave in a small stainless steel boat that was attached to the top of the autoclave with a stainless steel wire (the stainless steel boat had millimeter-sized holes on it to enhance the free exchange of the upper fluid and the lower fluid in the autoclave). De-aerated distilled water was used to fill the autoclave to 90–95% of its capacity. The resulting reaction solution usually had a pH value of 13–14. The autoclave was then tightly closed. The heating process for preparation of FeMgAl tochilinite was different from that of TSI. When preparing FeMgAl tochilinite, the autoclave was heated to 105 °C for 40–60 days and then the autoclave was allowed to cool naturally. However, when preparing TSI, the autoclave was first heated to 105 °C for 15–25 days. The electric stove was then turned off, and the autoclave was allowed to cool to room temperature. After that, the autoclave was kept at room temperature for another 10–15 days. Alternatively, a gradual decrease in temperature (e.g. from 105 °C to room temperature in 30 days) was also used to prepare TSI.

Both kinds of heating processes were carried out in a quiet environment with stable temperature, and vibration and shaking of the autoclave was strictly prohibited. Any leakage from the autoclave was avoided. After the heating process, the autoclave was carefully opened. The solid in the boat was first separated from the reaction solution and then collected. Later, we will refer to the solid in the boat as the heavy part of the product, because it settled quickly in water. The reaction solution from the autoclave was then poured into a 1 L beaker that formerly contained 800 mL distilled water. The liquid in the beaker was stirred for 10 min and then allowed to stand still for 50 min. A thin layer of dark material precipitated at the bottom of the beaker and some floccules remained suspended in the liquid. The liquid and the floccules were removed by decanting. We refer to this precipitate as the light part of the product, because it settled slowly in water. Both parts of the product were then washed with distilled water and a small amount of dilute hydrochloric acid (pH 5.8) until the filter liquor became neutral (acid-washing should be carried out carefully, as both parts are sensitive to acids of $pH < 4$). After that, they were rinsed with absolute ethanol and dried in a vacuum at 45 °C for 2–3 h. Both parts of the product were gray to black solids that could be attracted by a magnet. Also, both parts were soft, greasy or wax-like materials. However, the heavy part, especially the heavy part of the TSI product, sometimes included hard particles, which we considered to be unreacted MPPM. The unreacted MPPM could be removed by ultrasonicating the heavy part of the product in water, then collecting the suspensions by filtering. The heavy part of an FeMgAl tochilinite or TSI product always had a higher content of nanotubes than did the light part.

Tables A2 and A3 in the Appendix summarize the experiments we performed in pursuit of the optimum reaction conditions for the preparation of FeMgAl tochilinite and TSI, respectively.

4. RESULTS AND DISCUSSIONS

4.1. FeMgAl tochilinite

4.1.1. Results

Under FE-SEM, the heavy part of an FeMgAl tochilinite product generally exhibits a flake-like morphology. Fig. 1 shows representative FE-SEM images of such a sample (from run No. 434 of Table A2). The sample contains both large flakes (Fig. 1a) and small flakes (Fig. 1b). Based on TEM and EDX analyses, the large flakes shown in Fig. 1a are generally not FeMgAl tochilinite flakes. The small flakes shown in Fig. 1b are probably FeMgAl tochilinite flakes. The FeMgAl tochilinite flakes usually have a wavy, curved or rolled morphology. As the yield of FeMgAl tochilinite nanotubes is usually low (Table A2), it is inconvenient to observe them by SEM (but they can be easily identified by TEM). Under FE-SEM, the light part of a FeMgAl tochilinite product generally has similar morphology to that of the heavy part.

Fig. 2 shows TEM images of the FeMgAl tochilinite nanotubes. Fig. 2a is the TEM image of a cluster of the nanotubes (from run No. 168 of Table A2). The diameters of the nanotubes usually vary between 50 and 80 nm, although some nanotubes with relatively large diameters also exist, as shown in Fig. 2b and c (Fig. 2b–d are not from a single sample). Most of the FeMgAl tochilinite nanotubes have cone-like shapes with small cone apex angles (Fig. 2b and c). However, some quasi-cones with larger apex angles are occasionally observed (Fig. 2b), and most likely, it is the rolling of the FeMgAl tochilinite flakes around structural defects that forms them. The nanotube in Fig. 2c has a wrapping sheet. The nanotube-like structure in Fig. 2d appears to be produced by curling of two edges of a platelet. Both Fig. 2c and d suggest that some of the FeMgAl tochilinite nanotubes are likely to have been formed by curling of the corresponding flakes.

Under TEM, the FeMgAl tochilinite flakes generally have morphologies similar to what Kakos et al. (1994) observed. The size of the FeMgAl tochilinite flakes is generally smaller than 1.5 μm, suggesting that the tochilinite flakes are unable to grow to large sizes under our synthetic experimental conditions.

Fig. 3a and b shows TEM and HRTEM images of a FeMgAl tochilinite nanotube, respectively (from run No. 167 of Table A2). The HRTEM image of the wall of the nanotube shows close similarity with those of Kakos et al. (1994). Fig. 3c and d shows TEM and HRTEM images of an FeMgAl tochilinite flake, respectively (from run No. 366 of Table A2). The HRTEM images of the FeMgAl tochilinite nanotubes show inferior crystallinity to those of the FeMgAl tochilinite flakes. The FeMgAl tochilinite exhibits 10.6–11.1 Å (average 10.8 Å) basal

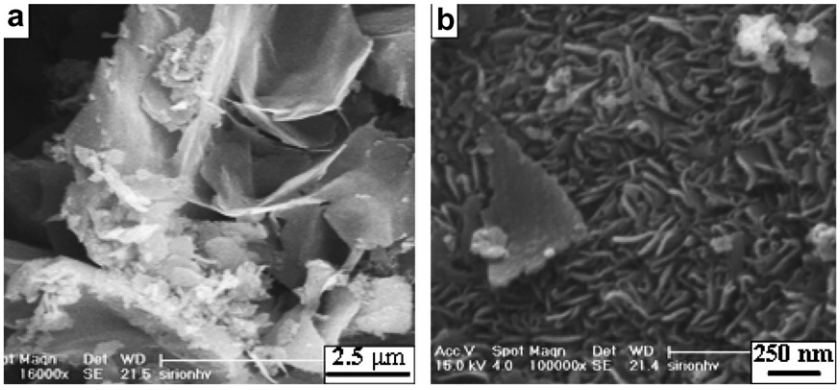

Fig. 1. Representative FE-SEM images of the heavy part of a FeMgAl tochilinite product. The heavy part contains both large flakes (a) and small flakes (b). The large flakes are generally not FeMgAl tochilinite flakes and the small flakes are probably FeMgAl tochilinite flakes.

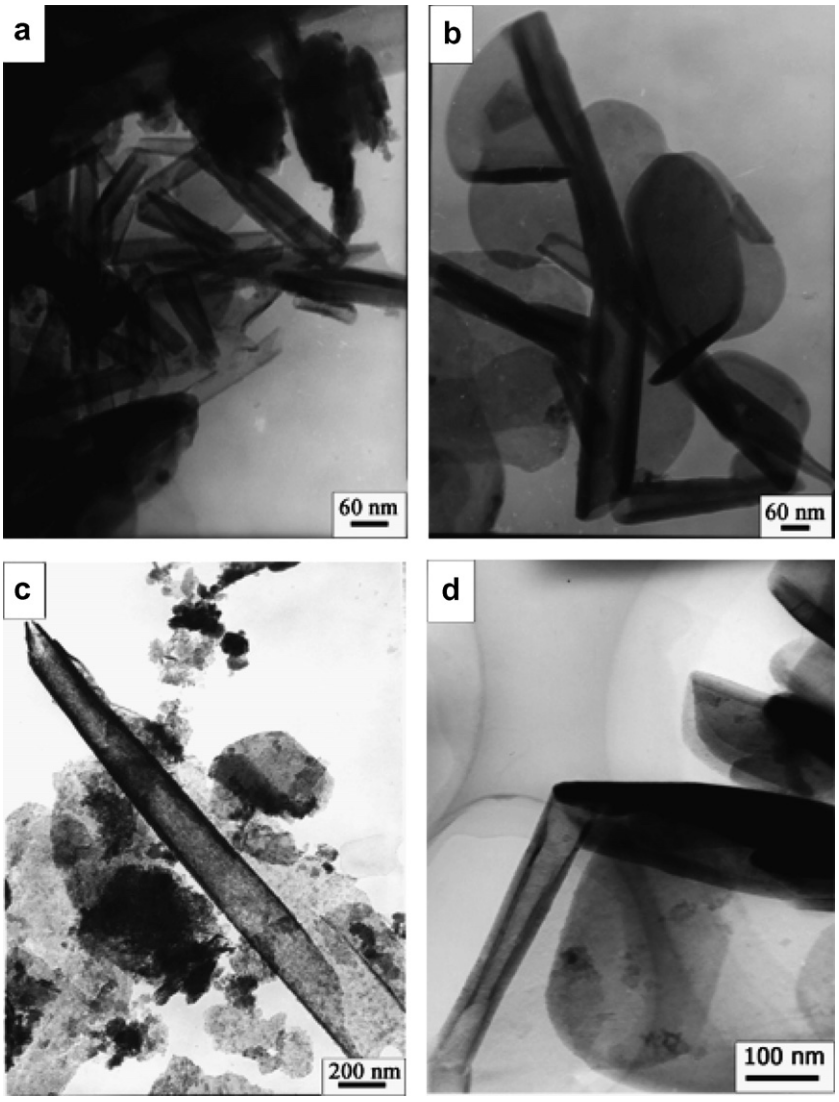

Fig. 2. Representative TEM images of FeMgAl tochilinite nanotubes: (a) a cluster of the nanotubes; (b) FeMgAl tochilinite nanotubes and rolled FeMgAl tochilinite flakes; (c) a nanotube with a wrapping sheet; (d) a nanotube-like structure that appears to be produced by curling of two edges of a platelet.

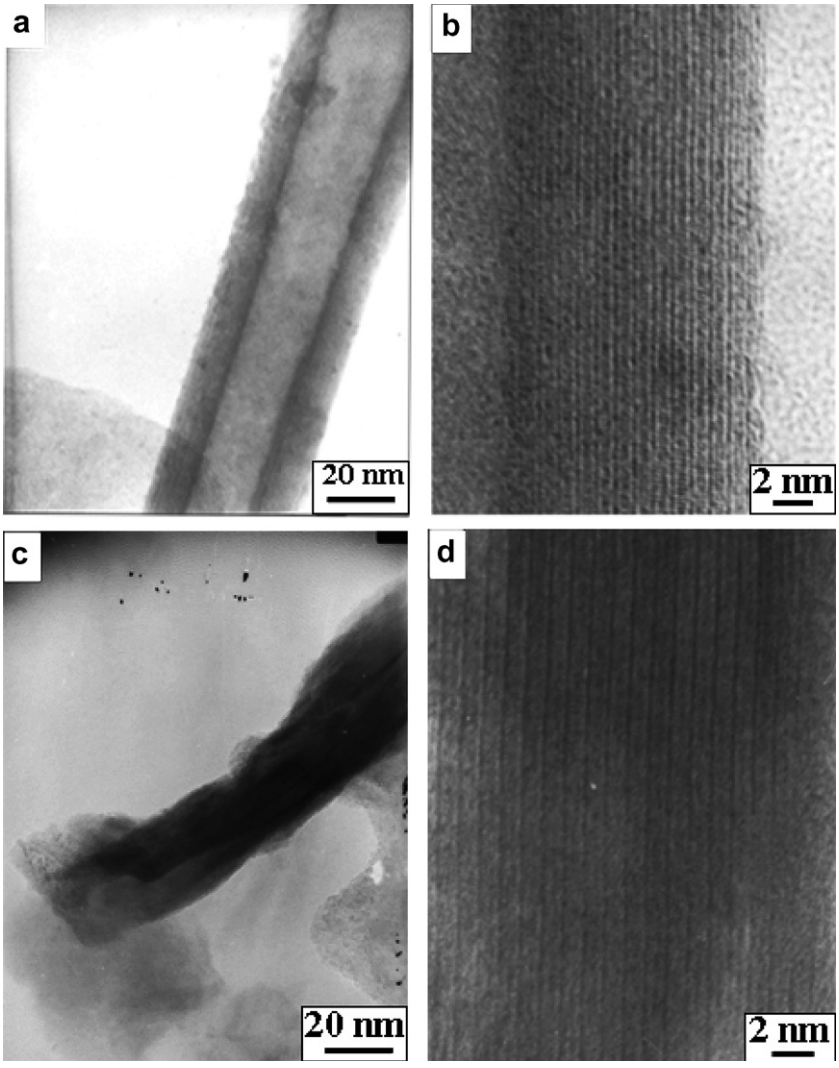

Fig. 3. (a and b) TEM and HRTEM images of an FeMgAl tochilinite nanotube, respectively; (c and d) TEM and HRTEM images of an FeMgAl tochilinite flake, respectively.

spacing along its *c*-axis (Fig. 3b and d), which agrees with that found in the literature data (Organova et al., 1974; Tomeoka and Buseck, 1983; Zolensky and Mackinnon, 1986; Kakos et al., 1994).

Due to poor crystallinity, only part of the thick-walled FeMgAl tochilinite nanotubes have relatively clear ED patterns, while thin-walled nanotubes have diffuse ED patterns. The crystallinity of the FeMgAl tochilinite flakes is slightly better than that of their nanotubes. However, it is important to note that, due to beam sensitivity, it is difficult to obtain both an HRTEM image and an ED pattern from a single FeMgAl tochilinite crystallite simultaneously. Fig. 4 shows representative ED patterns of FeMgAl tochilinite nanotubes and flakes. The main feature of these ED patterns is that almost all the ED patterns are composed of two sets of diffractions: one sharp and strong (probably originating from the sulfide layers of FeMgAl tochilinite) and the other weak and diffuse (probably produced from the hydroxide layers; Organova et al., 1974; Hughes et al., 1993; Kakos et al., 1994). Rotational twinning is also common for both the sulfide and the hydroxide layers. The FeMgAl tochilinite nanotubes usually have valleriite-like ED patterns (Fig. 4a and b) (from run No. 177 and 366 of Table A2), like those reported in the works of Hughes et al. (1993) and Kakos et al. (1994). The average lattice parameters of these nanotubes are: the sulfide layer $a_S = b_S = 3.6–3.8$ Å, and the hydroxide layer $a_H = b_H = 3.0–3.1$ Å, and $c = 10.6–11.1$ Å. The 0 0 1 diffractions of the nanotubes are strong and sharp, suggesting well-ordered interlayer structure. Some of the ED patterns of the FeMgAl tochilinite nanotubes show splitting of 0 0 1 spots, but the split spot distances are usually small (Fig. 4a). The split of the 0 0 1 diffractions also appears in the ED patterns of other kinds of conical nanotubular structures (Bernaerts et al., 1997; Yada and Iishi, 1977).

Chirality seems to be a common character of the FeMgAl tochilinite nanotubes (Margulis et al., 1996; Bernaerts et al., 1998; Xu et al., 2006). Fig. 4a is consistent with the ED patterns of helical or multi-helical nanotubes. The ED pattern in Fig. 4b shows a 30° chiral angle and the

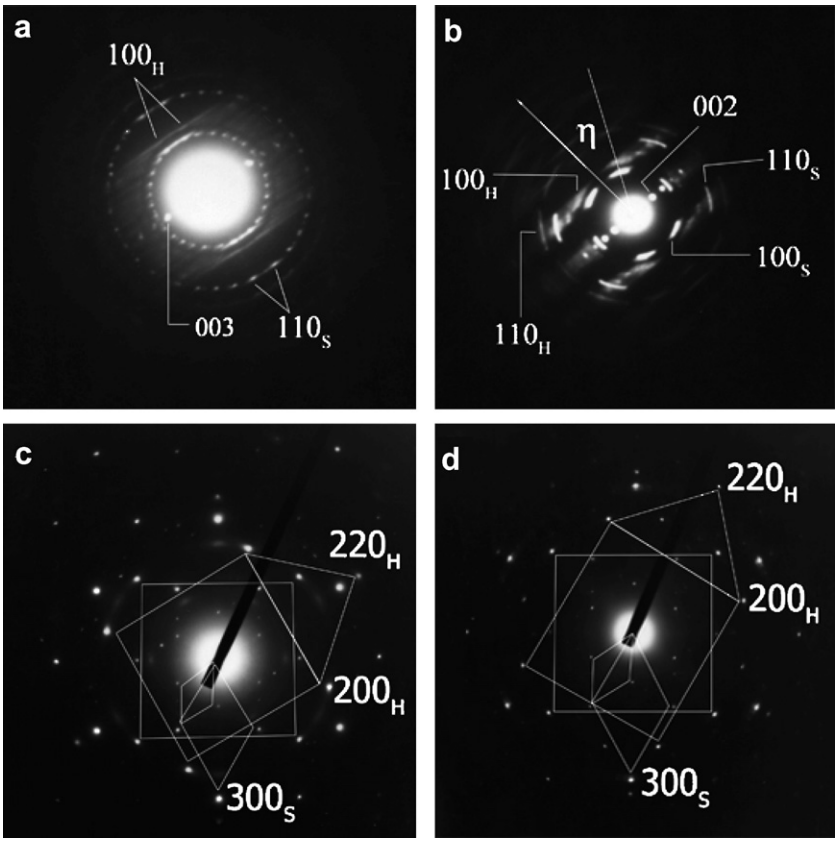

Fig. 4. (a and b) Representative ED patterns of FeMgAl tochilinite nanotubes, the chiral angle η in (b) is 30°; (c and d) representative ED patterns of FeMgAl tochilinite flakes.

layers made up of the nanotube seem to have small-angle rotational twinning.

FeMgAl tochilinite flakes prepared at high temperature but with a short reaction time (e.g. run No. 2 and No. 47 of Table A2) usually have valleriite-like ED patterns. However, with increased reaction time and decreased reaction temperature, the FeMgAl tochilinite flakes exhibit new ED patterns along with the valleriite-like ED patterns. These new ED patterns usually give larger a_S, b_S, a_H and b_H values than do the valleriite-like ones, whereas the c values remain constant. Fig. 4c and d shows two of these new ED patterns (from run No. 434, 366 of Table A2), which have relatively sharp diffraction spots. The main feature of the two ED patterns is that the diffractions from the sulfide layers are hexagonal, while those from the hydroxide layers are pseudo-tetragonal. The lattice parameters of the two ED patterns are summarized as:

$$\text{Fig. 4c}: a_S = b_S = 5.3\ \text{Å}, \quad a_H = b_H = 3.7\ \text{Å}$$

$$\text{Fig. 4d}: a_S = b_S = 5.1\ \text{Å}, \quad a_H = b_H = 3.7\ \text{Å}$$

The diffractions of the hydroxide layers in Fig. 4c and d all show 30° rotational twinning. The diffraction rings of the hydroxide layers in Fig. 4d are composed of 12 spots, each separated by 30°. Those in Fig. 4c are composed of 8 spots, which make up two rectangles rotated with respect to each other by 30°.

Table 1 shows representative EDX results of the FeMgAl tochilinite nanotubes. As oxygen and hydrogen as elements cannot be accurately measured by EDX, they were determined by difference. Analysis a is from a rare nanotube identified in the light part of a FeMgAl tochilinite product. Analyses b–d are EDX results of common FeMgAl tochilinite nanotubes identified in the heavy parts of FeMgAl tochilinite products. First, many of the EDX spectra of FeMgAl tochilinite nanotubes exhibited Fe/S atomic ratios smaller than 1, but varying between 0.6 and 0.9, as also observed by Kakos et al. (1994). However, Fe/S atomic ratios larger than 1 also made up a significant portion of the nanotubes (analysis c; also reported by Organova et al., 1974). Secondly, the EDX spectra show that Si can be a

Table 1
Representative EDX results of the FeMgAl tochilinite nanotubes

Element	*a* (wt%[a])	*b* (wt%)	*c* (wt%)	*d* (wt%)
Mg	16.1	12.1	12.5	10.1
Al	8.7	7.1	3.7	5.4
Si		1.8		1.0
S	15.4	20.9	20.2	24.5
Cr				1.9
Fe	20.1	29.8	36.1	32.0
Ni				1.3
O + H[b]	39.7	28.3	27.5	23.8
Total	100.0	100.0	100.0	100.0

[a] wt, weight.
[b] The O + H was determined by difference.

component of some FeMgAl nanotubes, though the content is not high (Si/Fe atomic ratio <0.17; analyses b and d). The FeMgAl tochilinite flakes generally are similar in composition to FeMgAl tochilinite nanotubes. However, the Fe/S atomic ratio of FeMgAl tochilinite nanotubes is always a little higher than their corresponding flakes, as also observed by Kakos et al. (1994). The Mg/Al atomic ratio of the EDX spectra normally varied between 0.8 and 2.5. It appears that very high concentration of Li^+ ions present in the reaction solution used to prepare FeMgAl tochilinite may have affected the Mg/Al atomic ratio (e.g. run No. 168 and 308 of Table A2), producing Mg/Al atomic ratios smaller than 1. However, like Na^+, diluted Li^+ ions would produce Mg/Al atomic ratios greater than 1 (e.g. run No. 309 of Table A2). Indeed, ICP-AES analysis of those samples synthesized in the presence of high concentrations of Li^+ ions revealed that a small amount of Li^+ ions was incorporated in the samples (the Li contents are usually smaller than 2%, w/w). Thus, we think that the FeMgAl tochilinite crystallites prepared with high concentrations of Li^+ ions probably contain some Li^+ ions as their component. This is understandable, given that the radius of a Li^+ ion (0.60 Å; Pauling ionic radius) is similar to that of a Mg^{2+} ion (0.65 Å) and so can substitute for Mg, lowering the Mg/Al ratio (the Li element cannot be detected by EDX). The Mg/Al atomic ratio does not have a great influence on the ED patterns of the FeMgAl tochilinite nanotubes and flakes, and thus it has little effect on the structure of the FeMgAl tochilinite in general. Given that the Mg/Al atomic ratio affects the determination of (Mg + Al)/Fe atomic ratio, it is better to synthesize FeMgAl tochilinite using a low concentration of Li^+ ions or by using Na^+ instead.

The (Mg + Al)/Fe atomic ratios from the EDX spectra of FeMgAl tochilinite nanotubes and flakes warrant special attention. The (Mg + Al)/Fe atomic ratios of analyses b–d in Table 1 agree with previously reported ratios of tochilinite, suggesting a 1:1 layer structure (1 brucite-like layer + 1 mackinawite-like layer; Organova et al., 1974; Kakos et al., 1994). The (Mg + Al)/Fe atomic ratio of analysis a in Table 1 is 2.7, which is twice the ratio of previously reported tochilinite. We think that the nanotube is probably made up of double brucite-like layers and single Fe–S layers (2 brucite-like layer + 1 mackinawite-like layer). However, we failed to obtain an HRTEM image or ED pattern of this nanotube. FeMgAl tochilinite flakes of the 2:1 phase have ED patterns similar to those of the 1:1 phase. We noticed that when the MPPM was not suspended in the autoclave but was placed at the bottom to prepare FeMgAl tochilinite (e.g. run No. 437 of Table A2), many FeMgAl tochilinite flakes of the 2:1 phase were produced.

The samples used in analyses a and c shown in Table 1 were obtained from Teflon-lined stainless steel autoclaves, whereas those of b and d were prepared using stainless steel autoclaves. The Si, Cr and Ni components in analyses b and d probably originated from the stainless steel autoclave (ingredients of the stainless steel autoclave were found to partly react in our experiment, however, their reaction speeds were much lower than those of the MPPM).

The XRD patterns of the FeMgAl tochilinite samples usually have poor quality (image not shown), with 10.6 Å (very weak) and 5.3 Å (strong) diffractions as the main feature of these XRD patterns. However, the XRD patterns of the FeMgAl tochilinite samples show close similarity to those of chondritic tochilinite (Nakamura and Nakamuta, 1996).

4.1.2. Discussion

Our synthetic FeMgAl tochilinite and natural tochilinites (terrestrial and chondritic) have the following similarities. The first is a compositional similarity. Some of the synthetic 1:1 FeMgAl tochilinite crystallites show an overall Fe/S atomic ratio larger than 1, similar to those of terrestrial tochilinite (analysis c in Table 1; Organova et al., 1974). Other 1:1 FeMgAl tochilinite crystallites have Fe/S atomic ratios smaller than 1, similar to those of the sulfide layers of terrestrial tochilinite (analyses b and d in Table 1). Considering the Mössbauer studies on the compositions of previously reported synthetic tochilinites (Kakos et al., 1994; Kozerenko et al., 1996, 2001; Rusakov et al., 1998; Chistyakova et al., 2005), the Fe/S atomic ratios, which to some extent reflect the distribution of Fe^{2+} ions in the sulfide layers and the hydroxide layers of tochilinite, and the overall compositions of the synthetic tochilinites, seem to be controlled by the ratios of the precursor metal ions. Thus, the Fe/S atomic ratios of some FeMgAl tochilinite crystallites smaller than 1 are probably caused by the high Mg and Al contents of our precursor MPPM, which suppress the occupancy of Fe^{2+} in the hydroxide layers of FeMgAl tochilinite (Rusakov et al., 1998; Chistyakova et al., 2005). Taking this viewpoint into consideration, we think that the overall compositions of our synthetic FeMgAl tochilinite exhibit similarity with those of natural tochilinites (Mackinnon and Zolensky, 1984; Tomeoka and Buseck, 1985; Zolensky and Mackinnon, 1986; Zolensky, 1987). The second similarity is that the lattice images of our synthetic 1:1 FeMgAl tochilinite (viewed along the direction perpendicular to the *c*-axis; Fig. 3b and d) are similar to those of natural 1:1 tochilinites (Tomeoka and Buseck, 1983, 1985; Zolensky and Mackinnon, 1986; Bradley and Brownlee, 1991). The third similarity is that the XRD patterns of the synthetic FeMgAl tochilinite show a remarkable resemblance to that of chondritic tochilinite (Nakamura and Nakamuta, 1996), though they show a significant intensity difference ($I_{10.8Å}$) compared to those of terrestrial tochilinite (Harris and Vaughan, 1972). The fourth similarity is morphology. Like terrestrial and chondritic tochilinite, the synthetic FeMgAl tochilinite exists in two forms: flakes and nanotubes (Figs. 1 and 2). The FeMgAl tochilinite flakes usually have wavy, curved, rolled, and sometimes straight morphology (Fig. 1), similar to natural tochilinites. The FeMgAl tochilinite nanotubes (Fig. 2) also show similarity to chondritic tochilinite nanotubes and terrestrial tochilinite microtubes.

Although the synthetic FeMgAl tochilinite shows the above similarities to both terrestrial and chondritic tochilinites, its XRD patterns and ED patterns (Fig. 4) suggest structural deviation from terrestrial tochilinite (Organova et al., 1974). The diffractions of the sulfide layers of the

FeMgAl tochilinite nanotubes and flakes usually have a hexagonal or pseudo-hexagonal symmetry, whereas those of the hydroxide layers usually have a hexagonal or pseudo-tetragonal symmetry (Fig. 4). These symmetries suggest structural deviation of the mackinawite-like and brucite-like sub-structures of our FeMgAl tochilinite from those of terrestrial tochilinite, respectively (Organova et al., 1974). This structural deviation may be due to several reasons, including the incorporation of a small amount of Li^+ or Na^+ ions into our FeMgAl tochilinite (Kozerenko et al., 2001), the high Al content, the strong reducing synthetic condition or the short reaction time (compared with geological time). The incorporation of Li^+ or Na^+ ions is probably caused by the high concentration of Li^+ or Na^+ ions in the reaction solution used to prepare FeMgAl tochilinite (Table A2). Thus, it is better to employ a less concentrated reaction solution of Li^+ or Na^+ ions to perform the hydrothermal synthesis to prepare terrestrial tochilinite. As there is no detailed structural information for chondritic tochilinite, we cannot make a comparison between our synthetic FeMgAl tochilinite and chondritic tochilinite. However, we tentatively conclude that the synthetic FeMgAl tochilinite is more like chondritic tochilinite than terrestrial tochilinite.

Many FeMgAl tochilinite flakes and all the FeMgAl tochilinite nanotubes have valleriite-like ED patterns (Fig. 4a and b). The valleriite-like ED patterns have a common characteristic, i.e. the dispersive diffraction spots or streaks originating from the sulfide and the hydroxide layers almost always tend to appear in pairs, which might indicate relatively strong interactions between structural units (or nanocrystalline islands) of the sulfide and the hydroxide layers (Hughes et al., 1993; Kakos et al., 1994). This kind of structural feature may be the reason that some FeMgAl tochilinite crystallites can contain tetrahedrally coordinated Si^{4+} as a component (analyses b and d in Table 1), even though normally Si^{4+} cannot exist in the octahedrally coordinated hydroxide layer of tochilinite (Organova et al., 1974). Some FeMgAl tochilinite crystallites can also incorporate Ni and Cr (analysis d in Table 1). Pure FeMgAl tochilinite crystallites (i.e. those which do not contain metal elements other than Fe, Mg and Al) were only obtained from Teflon-lined stainless steel autoclaves. These phenomena highlight the considerable compositional flexibility encompassed by the tochilinite structure.

Along with the increase in reaction time (Table A2), some of the valleriite-like ED patterns transform into new ED patterns of larger a_S, b_S, a_H and b_H values (Fig. 4c and d), which may be a reflection of tochilinite structure's two-dimensional incommensurability. The ED patterns shown in Fig. 4 may be considered to be ED patterns of metastable tochilinite in comparison with natural tochilinite.

Our FeMgAl tochilinite samples usually have poor XRD patterns, which may be due to the following reasons. The first is the low crystallinity of our FeMgAl tochilinite crystallites, as evidenced by ED analysis. The second is sample heterogeneity, as the FeMgAl tochilinite samples usually contain less than 50% of FeMgAl tochilinite crystallites (Table A2). The third is stoichiometry heterogeneity. Many of the FeMgAl tochilinite nanotubes and flakes of a single sample have different stoichiometries, and stoichiometry fluctuation sometimes occurs across a single FeMgAl tochilinite flake. The forth is two-dimensional incommensurability, which results in variable lattice parameters (Fig. 4).

Based on ICP-AES and EDX analyses, the heavy parts of FeMgAl tochilinite products contain higher amounts of Fe than do the light parts. As both parts are from the reaction of the original MPPM, the higher Fe content of the heavy parts indicates that reaction segregation did occur. This is understandable as the reaction is to some extent a hydrolysis process and the releasing speeds of Mg^{2+} and Al^{3+} ions from the FeMgAl tochilinite MPPM are probably higher than that of the Fe^{2+} ions. One conclusion derived from reaction segregation is that the yield of FeMgAl tochilinite is closely related to the size of the MPPM particles (size effect), with smaller MPPM particles (e.g. nanometer scale) having lower degrees of reaction segregation (the ingredients of nanometer scale MPPM would react quickly and similarly). Other conclusions are (1) the degree of reaction segregation is related to the reaction temperature, with low reaction temperatures having higher degrees of reaction segregation (temperature effect), (2) the FeMgAl tochilinite nanotubes prefer to form in a Fe-rich environment; hence, increasing the Fe/(Mg + Al) atomic ratio of the MPPM is a better way to increase the yield of FeMgAl tochilinite nanotubes, and (3) we should have used the elemental ratios of the FeMgAl tochilinite reported by Kakos et al. (1994) to prepare the MPPM and we should not have increased the Mg and Al contents.

The morphologies of the nanotubes in Fig. 2b–d and the ED pattern in Fig. 4a seem to support the general rolling mechanism of nanotube formation, as suggested by Yada and Iishi (1977) and Bernaerts et al. (1997) for mixed layer compounds. The various chiral angles of the FeMgAl tochilinite nanotubes indicate that the direction of the rolling of the layers is largely random (Margulis et al., 1996). However, this rolling process may be very delicate, as the hydrothermal preparation of FeMgAl tochilinite nanotubes requires a quiet reaction environment with stable temperature and pressure and without vibration.

Our experiments show that the FeMgAl tochilinite nanotubes prefer to form at low temperature. Experiments carried out at temperatures higher than 200 °C produce little tochilinite, usually without nanotubes (perhaps due to turbulent reaction solutions at high temperatures). Simply increasing the reaction temperature cannot improve the crystallinity of FeMgAl tochilinite greatly, and therefore, it is better to employ a relatively long reaction time and low reaction temperature. The FeMgAl tochilinite nanotubes can be better prepared at a temperature range of 90–105 °C (Table A2). However, the optimum reaction temperature is closely related to the size of the MPPM particles, with smaller MPPM particles (e.g. nanometer scale) requiring lower optimum reaction temperatures.

We found that if alkaline metal ions did not exist in the reaction system and only NH_4^+ ions (even if some $N_2H_4{\cdot}H_2O$ was also present) were used to sustain a basic environment, FeMgAl tochilinite was difficult to form (e.g. run No. 373 of Table A2). Na^+ or Li^+ ions were found to be necessary for the formation of FeMgAl tochilinite in

our reaction, while NH_4^+ ions did not have this ability. The Na^+ and Li^+ ions in our reaction may be able to affect the hydrolysis speeds of the ingredients of the MPPM and adjust the solubility of Al^{3+}, Mg^{2+} and Fe^{2+} ions, and thus, the transportation of them.

4.2. Tochilinite–serpentine-intergrowth (TSI)

4.2.1. Results

The heavy part of a TSI product is composed of particulate aggregates. Under FE-SEM, these particulates have a very porous appearance at low magnification. However, under high magnification, the particulates are covered by areas of different morphologies i.e. nanotube-rich regions, flake-rich regions and other undefined regions. Fig. 5a shows an FE-SEM image of a nanotube-rich region of a TSI sample (from run No. 436 of Table A3). The nanotube-rich region is composed of well defined and densely packed TSI nanotubes plus a minor amount of flakes. The nanotubes and the flakes grow directly on the surface of the original MPPM particles (in situ growth). Fig. 5b shows an FE-SEM image of some large platy, prism-like or rod-like materials that grow intimately with the TSI nanotubes and flakes; the image is from the same sample as Fig. 5a. Fig. 5c and d shows FE-SEM images of well formed and less densely packed TSI nanotubes and flakes (from run No. 266 of Table A3). It is apparent that many of the nanotubes have a relatively round cross section (Fig. 5c and d), although some nanotubes with quasi-rectangular cross sections (image not shown) and oval cross section have also been observed (Fig. 5d). Some nanotubes also have very small inner diameters (e.g. 7–9 nm; Fig. 5c).

Fig. 5e and f shows FE-SEM images of the flake-rich regions of TSI samples (Fig. 5e and f are from run No. 266 and 436 of Table A3, respectively). It is apparent that many of the densely packed flakes are quasi-rolled. Fig. 5e (left

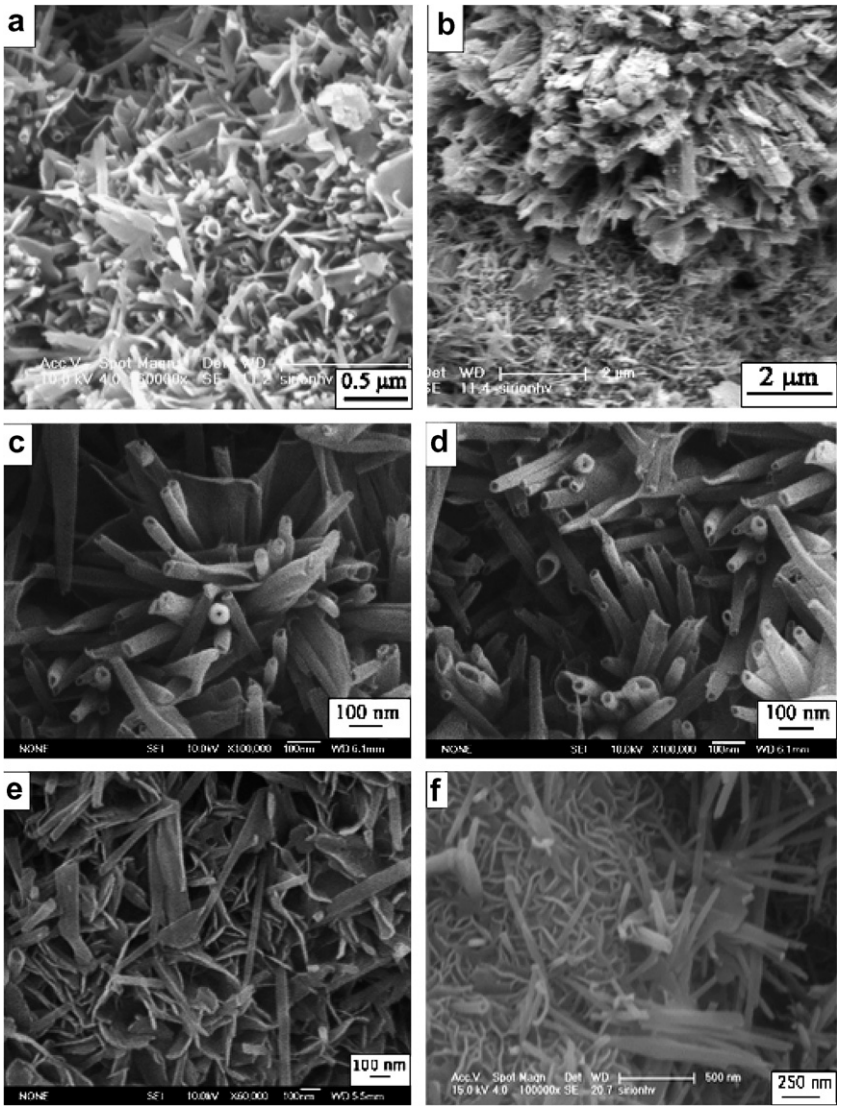

Fig. 5. Representative FE-SEM images of the heavy parts of TSI products: (a) a nanotube-rich region of a TSI sample; (b) FE-SEM image of some large platy, prism-like or rod-like materials that grow intimately with TSI nanotubes and flakes; (c,d) well formed and less densely packed TSI nanotubes and flakes; (e,f) flake-rich regions of TSI samples, the rod-like materials in (f) are intimately grown TSI nanotubes.

part), shows a nanotube that grows together with these flakes. The rod- and flake-like materials lying on the top of the densely packed flakes in Fig. 5e are probably TSI nanotubes and TSI flakes, respectively. Fig. 5f shows densely packed flakes closely associated with TSI nanotubes. The nanotubes shown here are growing at the less densely packed boundary region.

Fig. 6 shows typical FE-SEM images of the light part of a TSI product (from run No. 436 of Table A3). The light parts of TSI products are generally composed of complex components i.e. flakes, nanotubes, plates, prism-like and rod-like materials, aggregates of ultrafine particles, etc.

TEM observation reveals that the diameters of the TSI nanotubes generally vary between 25 and 70 nm. However, nanotubes with smaller and larger diameters were also observed. Compared with FeMgAl tochilinite nanotubes, the TSI nanotubes generally look longer and thinner. Fig. 7 shows representative TEM images of the TSI nanotubes and flakes (from run No. 436 and 450 of Table A3). The TSI nanotubes and flakes are inclined to grow into clusters and Fig. 7a shows a TEM image of such a cluster. Although the TSI nanotubes in Fig. 7a show a radiative-like morphology, careful examination reveals that the nearby nanotubes tend to be aligned parallel to their axes. Fig. 7b shows three

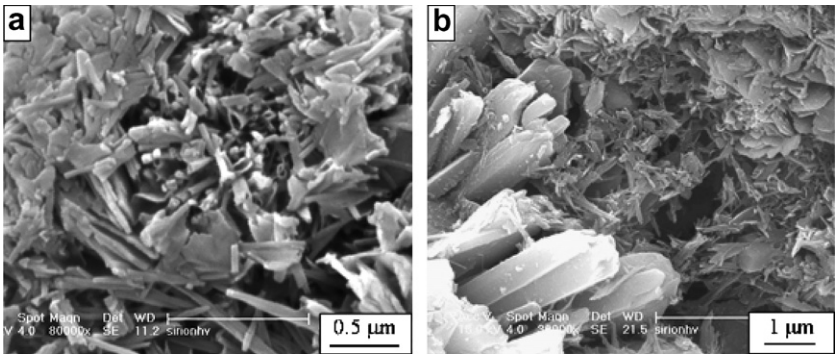

Fig. 6. Typical FE-SEM images (a,b) of the light part of a TSI product.

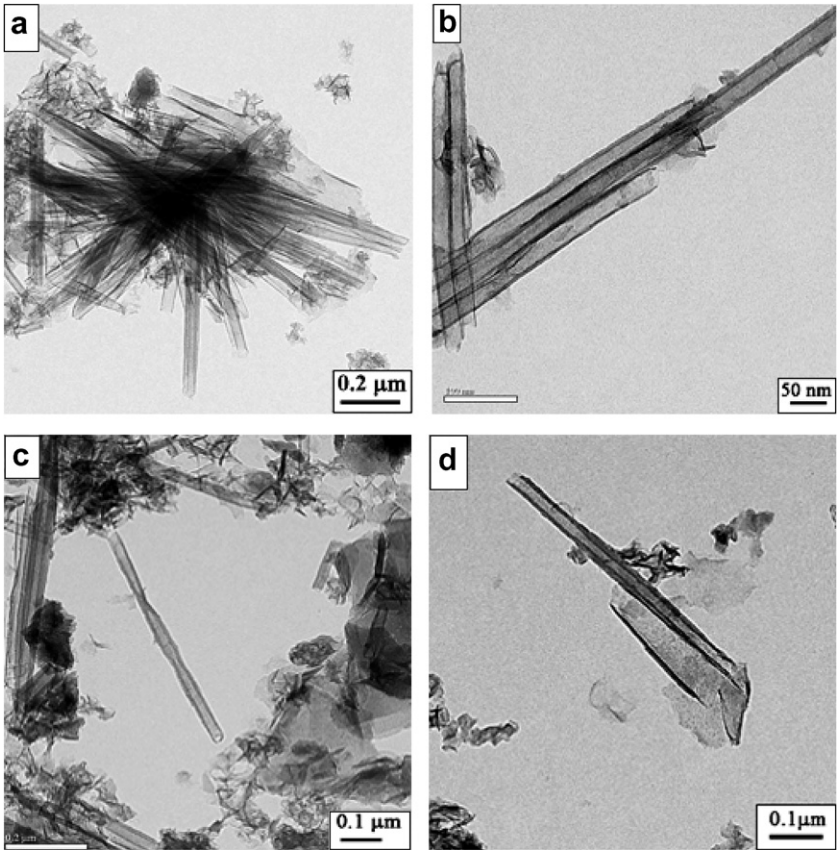

Fig. 7. Representative TEM images of the TSI nanotubes: (a) a TSI nanotube cluster; (b) typical parallel-growth mode of TSI nanotubes; (c) a thin-walled TSI nanotube with two diameter shrinkages along the tube axis, the conspicuously large shrinkage was caused by EDX analysis, while the smaller one was produced by ED recording; (d) a TSI nanotube closely associated with a rolling TSI flake.

parallel-growth TSI nanotubes. This kind of growth is typical of the TSI nanotubes and TSI flakes. Fig. 7c shows a thin-walled TSI nanotube with two diameter shrinkages along the tube axis. The conspicuously large shrinkage was caused by EDX analysis, while the smaller one was produced by ED recording. Both shrinkages demonstrate to some degree how sensitive the TSI nanotubes are toward the electron beam. Fig. 7d shows a TSI nanotube closely associated with a rolling TSI flake. Many of the TSI flakes are elongated along one direction (Fig. 7a, upper part; and Fig. 7d).

Fig. 8a and b shows TEM and HRTEM images of a TSI nanotube (from run No. 266 of Table A3), respectively. The TSI nanotube is not a perfect nanotube: it has relatively good crystallinity. Fig. 8c and d shows TEM and HRTEM images of a rolled TSI flake (from run No. 266 of Table A3), respectively. Like FeMgAl tochilinite nanotubes, the HRTEM images of TSI nanotubes show crystallinity inferior to the corresponding TSI flakes. The TSI crystallites usually have a 17.1–17.6 Å (average 17.4 Å) basal spacing along the **c**-direction, which is further composed of 10.2 Å (5.1 Å + 5.1 Å) and 7.2 Å spacings (Fig. 8b and d), suggesting a 1:1 intergrowth of serpentine-type layers and tochilinite-like layers (a $S–T_{1:1}–S–T_{1:1}$ intergrowth mode; $T_{1:1}$ represents 1:1 tochilinite). The $S–T_{1:1}–S–T_{1:1}$ intergrowth mode is the most frequently observed growth mode; however, other irregular intergrowth modes, like $S–T_{1:1}–S–T_{1:1}–T_3$ mode (T_3 represents a three-layer tochilinite), are also occasionally observed among TSI flakes (image not shown). The HRTEM images of our synthetic $S–T_{1:1}–S–T_{1:1}$ TSI nanotubes and flakes (Fig. 8b and d) are similar to those of previously reported natural 1:1 TSI (Tomeoka and Buseck, 1983, 1985; Mackinnon and Zolensky, 1984; Zolensky et al., 1993). However, the basal spacing of our $S–T_{1:1}–S–T_{1:1}$ TSI crystallites (average 17.4 Å) is smaller than that of natural 1:1 TSI (17.8 Å). Although TSI is an intergrowth of serpentine and tochilinite, on many occasions, this intergrowth is incomplete and some regions of certain TSI crystallites exhibit only the 7.2 Å fringes, as shown in the framed part in Fig. 8e (from run No. 355 of Table A3). Fig. 8f is an enlarged image of the framed part of Fig. 8e, showing the growth of only 7.2 Å fringes. We also observed that some areas of our TSI flakes contained only the 10.2 Å fringes; however, these areas usually blurred quickly precluding clear photo imaging. This incomplete intergrowth appears to be a recurring phenomenon of our TSI crystallites.

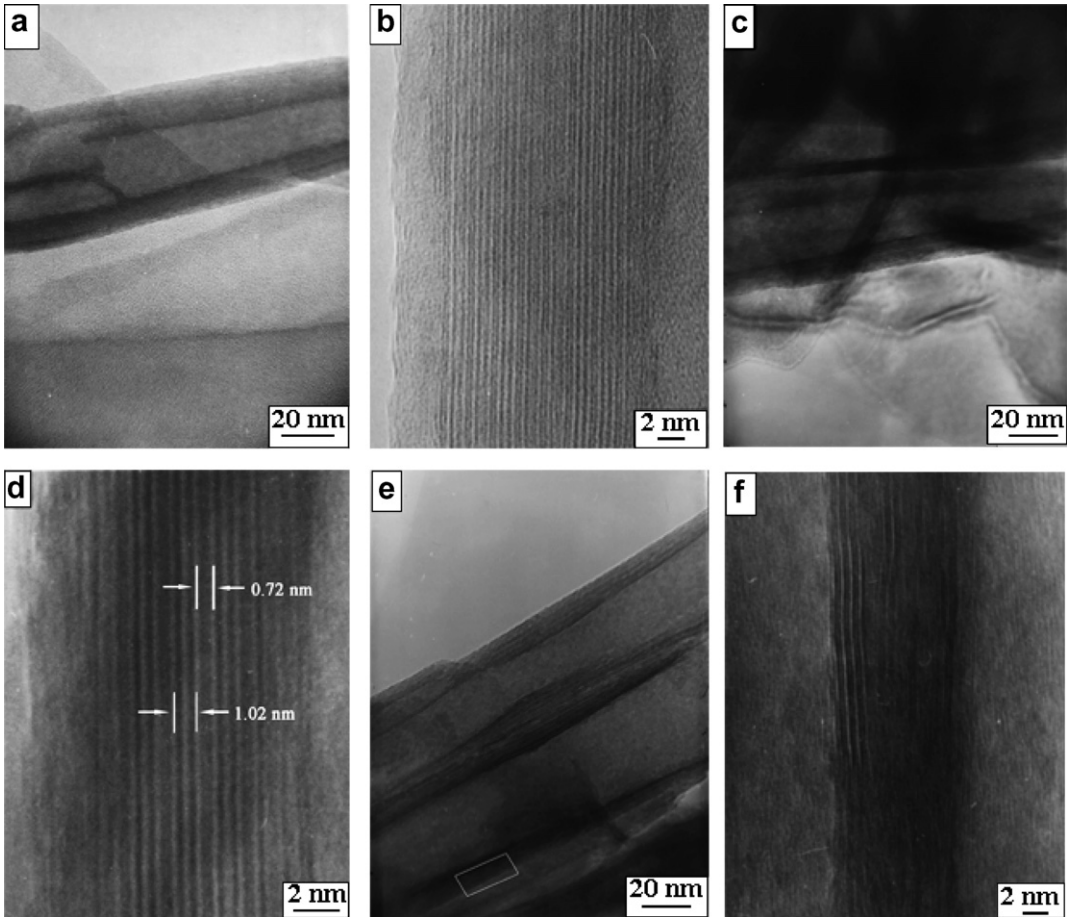

Fig. 8. (a and b) TEM and HRTEM images of a TSI nanotube, respectively; (c and d) TEM and HRTEM images of a rolled TSI flake, respectively; (e) TEM image of a rolled TSI flake, the framed part shows the incomplete intergrowth region of serpentine and tochilinite; (f) enlarged image of the framed part of (e), showing the growth of only 7.2 Å fringes.

Table 2
Representative EDX results of the TSI nanotubes

Element	*a* (wt%[a])	*b* (wt%)
Mg	7.6	3.9
Al	6.8	5.2
Si	6.3	6.9
S	9.8	10.5
Fe	26.9	34.8
O + H[b]	42.6	38.7

[a] wt, weight.
[b] The O + H was determined by difference.

Table 2 shows representative EDX results of TSI nanotubes. The most prominent feature of the EDX spectra of TSI nanotubes is their high Fe/S atomic ratio. The Fe/S atomic ratio is usually higher than 1.5 and varies between 1.5 and 5.3. However, sometimes it approaches 8.4. The Fe/Si atomic ratio usually ranges from 1.5 to 3.8. The Mg/Al atomic ratio varies between 0.8 and 1.5. Very concentrated Li^+ ions in the reaction solution used to prepare TSI can affect the Mg/Al atomic ratio (e.g. run No. 266 of Table A3), as previously discussed. The Mg/Al atomic ratio does not have great effect on the ED patterns of TSI nanotubes. The EDX spectra of TSI flakes are generally similar to those of TSI nanotubes.

Fig. 9 shows representative ED patterns of TSI nanotubes and TSI flakes. Most of our TSI nanotubes and flakes are amorphous, and only a trace amount of thick-walled TSI nanotubes and flakes had relatively clear ED patterns. Fig. 9a is the ED pattern of a well-formed TSI nanotube (from run No. 255 of Table A3), which can be indexed to a single hexagonal unit cell with lattice constants $a = b = 5.1$ Å, $c = 17.4$ Å. The 0 0 1 diffractions from the wall of the nanotube (parallel to the electron beam) are 8.7 Å (002), 5.8 Å (003, strongest), 4.3 Å (004) and 3.5 Å (005), similar to (but smaller than) the calculated diffractions of Fe–Si-only TSI by Nakamura and Nakamuta (1996). The c value of this nanotube suggests that it is an S–$T_{1:1}$–S–$T_{1:1}$ TSI nanotube. Fig. 9b is the ED pattern of a TSI nanotube with relatively poor crystallinity (from run No. 436 of Table A3). The 0 0 1 diffractions in Fig. 9b are diffuse and cannot be determined. However, the $hk0$ diffractions are clear and can be indexed to a single hexagonal unit cell with lattice constants $a = b = 5.7$ Å. The general features of Fig. 9a and b agree with the ED patterns of chrysotile nanotubes (Jancar and Suvorov, 2006). Fig. 9c is the ED pattern of a nanotube, which we cannot positively identify as TSI or tochilinite. The ED pattern has a pseudo-hexagonal symmetry and approximate lattice constants $a = b = 4.3$ Å, $c = 16.5$ Å. The c value of this nanotube is smaller than that of the S–$T_{1:1}$–S–$T_{1:1}$ TSI nanotube (17.4 Å). However, the EDX spectrum of this nanotube agrees with those of normal TSI nanotubes. It appears that this nanotube may be an intermediate between tochilinite and TSI or it may be an intergrowth of certain unknown

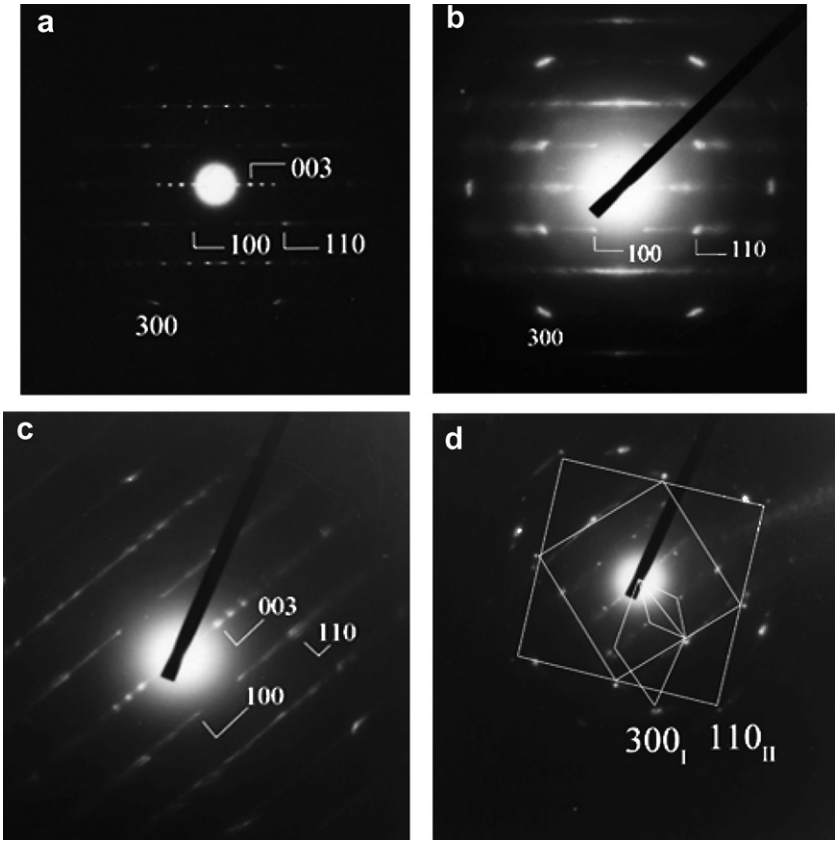

Fig. 9. Representative ED patterns of: (a,b) normal TSI nanotubes; (c) a rare TSI nanotube; (d) a TSI flake.

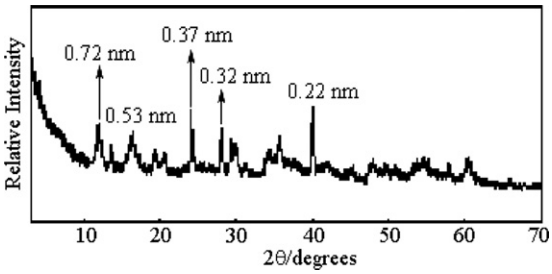

Fig. 10. Representative XRD pattern of a TSI complete sample.

layered silicate and mackinawite-like layers, rather than being an intergrowth of serpentine and tochilinite. The ED patterns in Fig. 9a–c can be classified as ED patterns of non-chiral nanotubes (Margulis et al., 1996; Bernaerts et al., 1998; Xu et al., 2006).

Fig. 9d is the ED pattern of a TSI flake near a TSI nanotube, as shown in Fig. 7d (some diffraction of the nanotube is inadvertently included in Fig. 9d). It is apparent that Fig. 9d resembles Fig. 9b. Fig. 9d shows two sets of diffractions, one is named diffraction-I, and the other diffraction-II. Diffraction-I has a pseudo-hexagonal symmetry with lattice constants $a_I = b_I = 5.8$ Å. Diffraction-II has a pseudo-tetragonal symmetry (depicted in Fig. 9d by rectangles) with lattice constants $a_{II} = b_{II} = 2.1$ Å. The lattice constants of diffraction-I are slightly larger than the lattice constants (5.7 Å) obtained from the ED pattern of Fig. 9b. The EDX spectrum of this flake shows that it has composition similar to those of TSI nanotubes; however, the Fe/S atomic ratio is slightly lower than that of normal TSI nanotubes.

A Representative XRD pattern of a TSI complete sample is shown in Fig. 10 (from run No. 367 of Table A3). The TSI complete sample is obtained by mixing the light part and the heavy part of a TSI product after the removal of the unreacted MPPM from the heavy part. The XRD patterns of the TSI samples are usually of poor quality. Fig. 10 shows a remarkable similarity to the XRD patterns of the matrices of some CM carbonaceous chondrites (Nakamura, 2005). Fig. 10 also shows a similarity to the XRD patterns of synthetic chrysotile (Foresti et al., 2005; Jancar and Suvorov, 2006), suggesting that chrysotile-like phases exist in our samples.

4.2.2. Discussion

Our synthetic TSI and natural TSI have the following similarities. The first is a compositional similarity. The Fe/S and Fe/Si ratios and the overall compositions of our synthetic TSI show great similarity to those of natural TSI (Table 2; Tomeoka and Buseck, 1983, 1985; Mackinnon and Zolensky, 1984; Zolensky and Mackinnon, 1986; Bradley and Brownlee, 1991; Zolensky et al., 1993). The second similarity is that the lattice images of our synthetic S–$T_{1:1}$–S–$T_{1:1}$ TSI (viewed along the direction perpendicular to the c-axis; Fig. 8b and d) are similar to those of natural 1:1 TSI. The incomplete interstratification of serpentine-type layers and tochilinite-like layers exhibited by our synthetic TSI (Fig. 8e and f) also show similarity to the incomplete intergrowth of cronstedtite and tochilinite of natural TSI. The third similarity is growth propensity. Like natural TSI (Tomeoka and Buseck, 1985), our synthetic TSI nanotubes and flakes like to grow into clusters, and the nanotubes in a single cluster always tend to arrange with their axes parallel (Figs. 5 and 7). Because of these similarities, we strongly suggest that at least part of the synthetic TSI samples are an intergrowth of cronstedtite and tochilinite.

The basal spacing of our S–$T_{1:1}$–S–$T_{1:1}$ TSI (17.4 Å) is smaller than both the basal spacings of natural 1:1 TSI (17.8 Å) and the theoretical Fe–Si-only TSI (18.0 Å; Nakamura and Nakamuta, 1996). The differences may be caused by the high Al content of our synthetic TSI (Table 2). The ionic radius of Al^{3+} ions (0.50 Å; Pauling ionic radius) is smaller than those of Mg^{2+} ions (0.65 Å) and Fe^{2+} ions (0.76 Å), and the incorporation of more Al^{3+} ions into the synthetic TSI structure may lead to the contraction of its basal spacing. This is a probable outcome, as the basal spacing of the FeMgAl tochilinite (10.6 Å, based on XRD data) is smaller than that of the Fe-only tochilinite (10.9 Å; Kozerenko et al., 1996). We attempted to verify this viewpoint by synthesizing the theoretical Fe–Si-only TSI, in order to obtain its basal spacing. Preliminary experimental results using Fe–Si alloy as the MPPM have verified that Fe–Si-only TSI nanotubes can exist, but they are extremely sensitive, both to air and to the electron beam, precluding detailed characterization presently. However, we found that some of the Fe–Si-only TSI nanotubes have diameters less than 10 nm (image not shown), much smaller than normal TSI nanotubes.

Considering the close relationship between the structure and composition of TSI flakes and TSI nanotubes (Fig. 7d, Fig. 9b and d), we suggest that some of the TSI nanotubes may have formed by curling of the TSI flakes along the direction perpendicular to the elongation of the TSI flakes. The non-chirality of many TSI nanotubes (Fig. 9a and b) supports unidirectional curling. The driving force of the curling may originate from TSI's misfit layer structure (Yada and Iishi, 1977; Bernaerts et al., 1997). The non-uniform ED patterns of TSI nanotubes (Fig. 9a and b) may be a kind of polymorphism. The hydrothermal synthesis of TSI nanotubes requires a quiet environment with stable temperature and pressure and without vibration, which indicates that the curling process is delicate (or the driving force is very weak). A post-heating low temperature treatment of the reaction (e.g. at room temperature or 0 °C) seems to be helpful in the formation of TSI nanotubes (e.g. run No. 255 and 266 of Table A3), which may be an intrinsic requirement of the TSI structure for nanotube formation or it could imply that a cooling process can make the densely packed TSI flakes less densely packed, thus facilitating the curling of the TSI flakes (Fig. 5e and f). It is also probable that the post-heating low temperature process can make the reaction solution supersaturated, which may be beneficial for the formation of TSI.

Like FeMgAl tochilinite, reaction segregation occurred in the hydrothermal synthesis of TSI mainly due to different releasing speeds of different metal ions from the TSI MPPM. The size effect and the temperature effect of reaction segregation discussed in Section 4.1.2 generally apply to the synthesis of TSI. Additional conclusions derived

from reaction segregation are: (1) the TSI nanotubes prefer to form in a Fe-rich environment, and so increasing the Fe/Mg, Fe/Al and Fe/Si atomic ratios of the TSI MPPM is a better way to increase the yield of TSI nanotubes; (2) we should have used the elemental ratios of TSI reported by Bradley and Brownlee (1991) to prepare the TSI MPPM and we should not have increased the Mg, Al and Si contents.

The discussions presented in Section 4.1.2 regarding sample heterogeneity, stoichiometry heterogeneity, reaction temperature and the functions of Li^+ and Na^+ ions generally apply to the synthesis of TSI.

5. SUMMARY OF THE EXPERIMENTAL RESULTS

FeMgAl tochilinite nanotubes and tochilinite–serpentine-intergrowth (TSI) nanotubes were hydrothermally prepared from metal particle precursor mixtures (MPPM) of (Fe + Mg + Al) and (Fe + Mg + Al + Si + Cr + Ni), respectively. The hydrothermal reaction was conducted below 200 °C under reducing and basic conditions. The reducing strength of the reaction system has a significant effect on the yield of FeMgAl tochilinite and TSI, especially their nanotubular forms. Reaction segregation always occurs during the hydrothermal reaction, mainly due to different releasing speeds of different metal ions from the MPPM. The morphologies, TEM and HRTEM images and compositions of our synthetic FeMgAl tochilinite and TSI show great similarity to natural tochilinite and TSI, respectively. The formation of the synthetic FeMgAl tochilinite nanotubes and TSI nanotubes requires a quiet reaction environment with stable temperature and pressure and without vibration, which suggests that natural tochilinite nanotubes and TSI nanotubes in CM carbonaceous chondrites may be formed under similar conditions. A deduction based on reaction segregation is that if our reaction was performed in a low gravitation environment and without other interferences, the Fe content around an original MPPM particle after the hydrothermal reaction would have a radial distribution, with outer layers having a lower content of Fe.

6. APPLICATIONS TO METEORITICS

6.1. Inferences for parent body alteration of CM chondrites

Based on our experimental work, we suggest that the precursors of tochilinite and TSI in the matrix and FGRs in CM carbonaceous chondrites may be aggregates of nanometer to micrometer scale metal particles (including alloy particles) of Fe, Mg, Si, Al, Ni, Cr, etc. These metal particles may have been formed in a locally reduced region in the solar nebula before accreting into the parent bodies of CM carbonaceous chondrites (see below). They probably underwent aqueous alteration in the parent bodies with S^{2-} bearing basic water (the pH value of the water probably varies between 8 and 10) under strongly reducing conditions. The reducing conditions could have been produced by the reaction of metal particles and S^{2-} bearing water. The labile structures of tochilinite and TSI and the delicate reaction conditions required for the production of tochilinite nanotubes and TSI nanotubes suggest alteration conditions similar to the reaction conditions of our experiments (i.e. a quiet reaction environment with stable temperature and pressure without vibration). The local Fe/Si ratio of the metal particle mixture may determine the production of tochilinite or TSI, as our experiments indicate. Of course, the production of tochilinite and TSI are also affected by the ratios of the various metals to S^{2-}, especially the ratio of Fe/S^{2-}. The alteration probably proceeds at relatively low temperature (e.g. 50–100 °C), which may be determined to some extent by the metal/water ratio and the chondrule/metal ratio of a parent body. However, due to the probable poor conductivity of the materials of the parent bodies of CM chondrites, the alteration temperature may differ at different sites of a parent body (e.g. interior and exterior). The alteration temperature may have a great effect on the evolution of the mineralogy of a parent body. If the alteration temperature is very low (e.g. 0 °C), due to reaction segregation, the yield of tochilinite and TSI will be low. If the alteration temperature is very high (e.g. >220 °C), the production of tochilinite and TSI, especially in their nanotubular forms, will be likewise inhibited.

The CM carbonaceous chondrites contain minerals like carbonates and sulfates (Zolensky et al., 1993) that seem to be formed only in an oxidizing environment. Although they may be plausible condensates from the canonical solar nebula, we think that other mechanisms should not be overlooked; it is probable that these minerals can also be produced in a reducing environment. For example, the series of works done by Huber and Wächtershäuser (1997, 1998, 2006) mimicking biological carbon fixation show that carbonates can be produced in a reducing environment employing carbon monoxide (CO), which is a ubiquitous component of the solar nebula, as the carbon source and iron sulfide and/or iron hydroxide as catalysts.

6.2. Inferences on production of metal particles in the solar nebula

According to the canonical theory of solar nebula, the nebula environment is sufficiently oxidizing to prohibit the existence of metallic Si, Mg and Al. However, systematic studies on various chondrites seem to suggest that highly reducing and high-temperature environments can exist locally in the solar nebula (Krot et al., 2000; Pack et al., 2004, 2005). Based on the framework of a recent model (or similar models) on chondrule and refractory inclusion formation (Shu et al., 1996, 2001; Gounelle et al., 2001), one possible site for such highly reducing and high-temperature environments is the inner nebula near the protosun (Rai et al., 2005). The highly reducing environments are probably produced by evaporation and pyrolysis of the carbonaceous materials (Krot et al., 2000). Such environments may begin to emerge at relatively late stages of nebular evolution, when H_2O is gradually transported into the outer nebula beyond the snowline (Krot et al., 2000; Ciesla and Cuzzi, 2006). The outward transport of H_2O leads to the enrichment of the inner solar accretion disk with carbonaceous materials (i.e. the C/O ratio of the accretion disk increases). As refractory inclusions are generally considered to have formed earlier in the solar nebula than were chond-

Table A1
The purity and size of the metal particles used to synthesize FeMgAl tochilinite and TSI

Properties	Elements					
	Fe	Mg	Al	Si	Cr	Ni
Purity	⩾98%	⩾99%	⩾99%	⩾99.9%	⩾99.95%	⩾99.5%
Size (mesh)	200	100–200	100–200	200	200	200

rules, the highly reducing environments probably appeared at the time of chondrule formation and afterwards (Pack et al., 2005). In the highly reducing and high-temperature environments, metal particles, like Fe, Si, Mg, and Al, may have been produced. Metal particles produced in the inner nebula could then be transported by the X-wind to the accretion sites of the CM chondrite parent bodies (Shu et al., 1996, 2001).

Table A2
Summary of hydrothermal experiments for preparing FeMgAl tochilinite

Run number and expt. times	MPPM (g)	NaOH (mmole)	$LiOH{\cdot}H_2O$ (mmole)	$(NH_4)_2S$ (mmole)	$N_2H_4{\cdot}H_2O$ (ml)	Temp. (°C)	Heating time (days)	Average yield
No. 1	0.3	0	15.4	7.06	0	220	4	0[a]
3 (S[b])								Trace[a]
No. 2	0.3	0	15.4	7.06	0	198	4	0
3 (T[b])								<6%
No. 7	0.3	0	7.0	7.06	0	198	4	trace
4 (S)								<6%
No. 9	0.3	0	0	7.06	0	198	4	0
4 (S)								0
No.14[c]	0.3	0	15.4	7.06	0	198	4	Trace
4 (S)								<8%
No. 47	0.3	0	15.4	5.80	3	198	6	<2%
6 (S)								<10%
No. 50	0.3	0	0	5.80	18	170	6	0
2 (T)								0
No. 54	0.3	15.4	0	5.80	18	105	50	<2%
5 (S)								<30%
No. 147	0.3	15.4	0	8.0	18	50	60	Trace
2 (S)								<30%

Run number and Expt. times	MPPM (g)	NaOH (mmole)	$LiOH{\cdot}H_2O$ (mmole)	S (mmole)	$N_2H_4{\cdot}H_2O$ (ml)	Temp. (°C)	Heating time (days)	Yield
No. 153	0.30	10.0	0	9.0	21	125	18	<2%
2 (S)								<30%
No. 167	0.30	10.0	0	9.0	21	105	18	<4%
2 (S)								<30%
No. 168	0.30	0	15.7	9.0	21	105	18	<7%
2 (S)								<40%
No. 177	0.30	15.7	0	9.0	20	150	5	<2%
2 (S)								<30%
No. 308	0.30	0	15.4	5.0	18	105	41	<1%
2 (S)								<20%
No. 309	0.30	0	5.0	8.0	12	105	41	<2%
2 (S)								<35%
No. 366	0.42	0	8.3	8.0	19	150	20	<1%
2 (T)								<35%
No. 434	0.42	10	0	9.0	19	105	50	<1%
2 (T)								<35%
No. 437	0.3	15.7	0	8	19	95	50	0
2[d] (T)								<30%

[a] The upper data shows the average yield (or content) of FeMgAl tochilinite nanotubes and the lower data shows the average yield of FeMgAl tochilinite flakes. The yields were determined after statistical analysis of the TEM and EDX characterization results of FeMgAl tochilinite complete samples (i.e. the heavy part + the light part). If a sample contains high amount of FeMgAl tochilinite nanotubes and FeMgAl tochilinite flakes, the yields would be relatively easy to determine. However, if it contains a low amount of FeMgAl tochilinite nanotubes and FeMgAl tochilinite flakes, the data determined would have errors, depending on one's estimation of the TEM images.

[b] S denotes stainless steel autoclaves, while T denotes Teflon-lined stainless autoclaves.

[c] The four experiments were performed by flushing the autoclaves with H_2 before closing them (for details, see text).

Table A3
Summary of hydrothermal experiments for preparing TSI nanotubes

Run number and expt. times	MPPM (g)	NaOH (mmole)	$LiOH{\cdot}H_2O$ (mmole)	S (mmole)	$N_2H_4{\cdot}H_2O$ (ml)	Temp. (°C)	Heating time (days)	Average yield
No. 255[b] 3	0.40	10.0	0	11	20	160	5	<7%[a]
No. 256[b] 3	0.40	10.0	0	11	20	160	5	<7%
No. 266[c] 2	0.42	0	15.4	11	20	105, 22	30	⩽35%
No.267 3	0.42	0	15.7	11	20	45	60	<3%
No.268 3	0.42	15.7	0	11	20	35	60	<6%
No.274 2	0.40	0	15.4	9.0	19	198	5	Trace
No. 355 2	0.40	0	10.0	8.0	20	105	35	8%
No.367 2	0.32	0	15.4	9.0	18	150	20	3%
No.376 2	0.30	0	0	8.0	18	98	30	0
No.391[d] 2	0.30	0	15.4	8.0	18	120	12	<5%
No.435 2	0.40	15.7	0	10.0	20	105	60	<5%
No.436[c] 3	0.42	10.0	0	9.0	20	105, 20	50	⩽15%
No. 439 2	0.40	10.0	0	8.0	19	45	120	3%
No.450[c] 2	0.42	0	15.4	9.0	20	105, 20	25	⩽10%

[a] The average yield (or content) of TSI nanotubes. The yield was determined after statistical analysis of the TEM and EDX characterization results of TSI complete samples (i.e. the heavy part + the light part).
[b] These experiments had a 4 day reaction time and a one day naturally cooling process, the environment temperature was about −4 °C.
[c] In these experiments, the autoclaves were first heated at 105 °C for 15–25 days. The electric stove was turned off and the autoclaves were allowed to cool to room.
[d] The two experiments were performed with a gradually decreasing reaction temperature.

ACKNOWLEDGMENTS

We are grateful to Dr. Eric Tonui (University of California, Los Angeles) and Dr. Sara Russell (The Natural History Museum, London) for their valuable comments and corrections to the English of the manuscript. Without their efforts, this paper may not have been accomplished in the present style. We are also grateful to two anonymous reviewers for their constructive comments, which helped improve the manuscript significantly. Y.P. thanks Ms. Yonggai Dong for her kind assistance in this work. This research was supported by Anhui Provincial Natural Science Foundation of China (to Y.P. under contract No. 03046302), China Postdoctoral Science Foundation (to Y.P.) and Zhengzhou University.

APPENDIX A

See Tables A1–A3.

REFERENCES

Bernaerts D., Amelinckx S., Van Tendeloo G., and Van Landuyt J. (1997) Microstructure and formation mechanism of cylindrical and conical scrolls of the misfit layer compounds $PbNb_nS_{2n+1}$. *J. Cryst. Growth* **172**, 433–439.

Bernaerts D., Amelinckx S., Lambin Ph., and Lucas A. A. (1998) The diffraction space of circular and polygonized multishell nanotubules. *Appl. Phys. A* **67**, 53–64.

Bradley J. P., and Brownlee D. E. (1991) An interplanetary dust particle linked directly to type CM meteorites and an asteroid origin. *Science* **251**, 549–552.

Browning L. B. and Bourcier W. L. (1996) Tochilinite: a sensitive indicator of alteration conditions on the CM asteroidal parent body. *Lunar Planet. Sci. XXVII*. Lunar Planet. Inst., Houston. #171 (abstr.).

Chistyakova N. I., Rusakov V. S., Gubaidulina T. V., and Kozerenko S. V. (2005) Investigations of sulfide minerals with layered structure by Mössbauer spectroscopy methods. *Hyperfine Interact.* **166**, 613–617.

Ciesla F. J., and Cuzzi J. N. (2006) The evolution of the water distribution in a viscous protoplanetary disk. *Icarus* **181**, 178–204.

Dódony I., and Buseck P. R. (2004) Serpentines close-up and intimate: an HRTEM view. *Int. Geol. Rev.* **46**, 507–527.

Evans H. T., and Allmann R. (1968) The crystal structure and crystal chemistry of valleriite. *Z. Kristallogr.* **127**, 73–93.

Foresti E., Hochella, Jr., M. F., Kornishi H., Lesci I. G., Madden A. S., Roveri N., and Xu H. F. (2005) Morphological and chemical/physical characterization of Fe-doped synthetic chrysotile nanotubes. *Adv. Funct. Mater.* **15**, 1009–1016.

Gounelle M., Shu F. H., Shang H., Glassgold A. E., Rehm K. E., and Lee T. (2001) Extinct radioactivities and protosolar cosmic rays: self-shielding and light elements. *Astrophys. J.* **548**, 1051–1070.

Harris D. C., and Vaughan D. J. (1972) Two fibrous iron sulfides and valleriite from Cyprus with new data on valleriite. *Am. Mineral.* **57**, 1037–1052.

Huber C., and Wächtershäuser G. (1997) Activated acetic acid by carbon fixation on (Fe, Ni)S under primordial conditions. *Science* **276**, 245–247.

Huber C., and Wächtershäuser G. (1998) Peptides by activation of amino acids with CO on (Fe, Ni)S surfaces: implications for the origin of life. *Science* **281**, 670–672.

Huber C., and Wächtershäuser G. (2006) α-Hydroxy and α-amino acids under possible Hadean, volcanic origin-of-life conditions. *Science* **314**, 630–632.

Hughes A. E., Kakos G. A., Turney T. W., and Williams T. B. (1993) Synthesis and structure of valleriite, a layered metal hydroxide/sulfide composite. *J. Solid State Chem.* **104**, 422–436.

Jancar B., and Suvorov D. (2006) The influence of hydrothermal-reaction parameters on the formation of chrysotile nanotubes. *Nanotechnology* **17**, 25–29.

Kakos G. A., Turney T. W., and Williams T. B. (1994) Synthesis and structure of tochilinite: a layered metal hydroxide/sulfide composite. *J. Solid State Chem.* **108**, 102–111.

Kogure T., Hybler J., and Durovic S. (2001) A HRTEM study of cronstedtite: determination of polytypes and layer polarity in trioctahedral 1:1 phyllosilicates. *Clays Clay Minerals* **49**, 310–317.

Kozerenko S. V., Organova N. J., Fadeev V. V., Magazina L. O., Kolpakova N. N., and Kopnev L. A. (1996) Tochilinite produced in laboratory. *Lunar Planet. Sci. XXVII*. Lunar Planet. Inst., Houston. #695 (abstr.).

Kozerenko S. V., Fadeev V. V., Organova N. I., Rusakov V. S., Chistyakova N. I., Kolpakova N. N., and Senin V. G. (2001) Synthesis, formation conditions and crystallochemistry of tochilinites-iron, magnesium and sodium hydroxide-sulfides. *Exp. Geosci.* **10**, 57–58. Available from: <http://library.iem.ac.ru/exper/v10_1/contents.html>.

Krot A.N., Fegley B., Lodders K., and Palme H. (2000) Meteoritical and astrophysical constraints on the oxidation state of the solar nebula. In *Protostars and Planets IV* (eds. V. Mannings, A. Boss, S.S. Russell). University of Arizona Press, Tucson, pp. 1019–1054.

Lennie A. R., Redfern S. A. T., Schofield P. F., and Vaughan D. J. (1995) Synthesis and Rietveld crystal structure refinement of mackinawite, tetragonal FeS. *Mineral. Mag.* **59**, 677–683.

Mackinnon I. D. R., and Zolensky M. E. (1984) Proposed structures for poorly characterized phases in C2M carbonaceous chondrite meteorites. *Nature* **309**, 240–242.

Margulis L., Dluzewski P., Feldman Y., and Tenne R. (1996) TEM study of chirality in MoS_2 nanotubes. *J. Microsc. (Oxford)* **181**, 68–71.

Mellor J. W. (1958) The chemical properties of hydrazine and its hydrates. In *A Comprehensive Treatise on Inorganic and Theoretical Chemistry*, vol. VIII (ed. G. D. Parkes). Longmans, Green and Co., London, New York, and Toronto. pp. 312–321.

Moroz L. V., Kozerenko S. V., and Fadeev V. V. (1997) The reflectance spectrum of synthetic tochilinite. *Lunar Planet. Sci. XXVIII*. Lunar Planet. Inst., Houston. #1288 (abstr.).

Nakamura T. (2005) Post-hydration thermal metamorphism of carbonaceous chondrites. *J. Mineral. Petrol. Sci.* **100**, 260–272.

Nakamura T., and Nakamuta Y. (1996) X-ray study of PCP from the Murchison CM carbonaceous chondrite. *Proc. NIPR Symp. Antarct. Meteorites* **9**, 37–50.

Organova N. I., Drits V. A., and Dmitrik A. L. (1974) Selected area electron diffraction study of a type II "valleriite-like" mineral. *Am. Mineral.* **59**, 190–200.

Pack A., Yurimoto H., and Palme H. (2004) Petrographic and oxygen-isotopic study of refractory forsterites from R-chondrite Dar al Gani 013 (R3.5-6), unequilibrated ordinary and carbonaceous chondrites. *Geochim. Cosmochim. Acta* **68**, 1135–1157.

Pack A., Palme H., and Shelley J. M. G. (2005) Origin of chondritic forsterite grains. *Geochim. Cosmochim. Acta* **69**, 3159–3182.

Rai V. K., Jackson T. L., and Thiemens M. H. (2005) Photochemical Mass-Independent Sulfur Isotopes in Achondritic Meteorites. *Science* **309**, 1062–1065.

Rusakov V. S., Chistyakova N. I., Kozerenko S. V., and Fadeev V. V. (1998) Mössbauer investigations of the synthetic tochilinites. *Lunar Planet. Sci. XXIX*. Lunar Planet. Inst., Houston. #1604 (abstr.).

Schöllhorn R., and Meyer H. (1974) Cathodic reduction of layered transition metal dichalcogenides. *Mat. Res. Bull.* **9**, 1237–1246.

Schöllhorn R., Sick E., and Lerf A. (1975) Reversible topotactic redox reactions of layered dichalcogenides. *Mat. Res. Bull.* **10**, 1005–1012.

Shu F. H., Shang H., and Lee T. (1996) Toward an astrophysical theory of chondrites. *Science* **271**, 1545–1552.

Shu F. H., Shang H., Gounelle M., Glassgold A. E., and Lee T. (2001) The origin of chondrules and refractory inclusions in chondritic meteorites. *Astrophys. J.* **548**, 1029–1050.

Tenne R., and Rao C. N. R. (2004) Inorganic nanotubes. *Phil. Trans. R. Soc. Lond. A* **362**, 2099–2125.

Tomeoka K., and Buseck P. R. (1983) A new layered mineral from the Mighei carbonaceous chondrite. *Nature* **306**, 354–356.

Tomeoka K., and Buseck P. R. (1985) Indicators of aqueous alteration in CM carbonaceous chondrites: microtextures of a layered mineral containing Fe, S, O and Ni. *Geochim. Cosmochim. Acta* **49**, 2149–2163.

Welz D., and Rosenberg M. (1987) Electronic band structure of tetrahedral iron sulphides. *J. Phys. C: Solid State Phys.* **20**, 3911–3924.

Xu Z., Bai X., Wang Z. L., and Wang E. (2006) Multiwall carbon nanotubes made of monochirality graphite shells. *J. Am. Chem. Soc.* **128**, 1052–1053.

Yada K., and Iishi K. (1977) Growth and microstructure of synthetic chrysotile. *Am. Mineral.* **62**, 958–965.

Zolensky, M. E. (1987) Tochilinite in C2 carbonaceous chondrites: a review with suggestions. *Lunar Planet. Sci. XVIII*. Lunar Planet. Inst., Houston. #1132 (abstr.).

Zolensky M. E., and Mackinnon I. D. R. (1986) Microstructures of cylindrical tochilinites. *Am. Mineral.* **71**, 1201–1209.

Zolensky M., Barrett R., and Browning L. (1993) Mineralogy and composition of matrix and chondrule rims in carbonaceous chondrites. *Geochim. Cosmochim. Acta* **57**, 3123–3148.

Associate editor: Sara S. Russell